Extracellular Vesicle 7 (2026) 100101

Contents lists available at ScienceDirect

Extracellular Vesicle

journal homepage: www.elsevier.com/locate/vesic

Discriminating extracellular vesicles by their membranes

Carlo Guardiani [a], Matteo Riboli [a], Flavio Costa [a], Massimiliano Bruno [a], Giulia Rossi [b], Alberto Giacomello [a,*]

[a] Dipartimento di Ingegneria Meccanica e Aerospaziale, Sapienza Università di Roma, Via Eudossiana 18, 00184, Rome, Italy
[b] Department of Physics, Università degli Studi di Genova, Via Dodecaneso 33, 16146, Genoa, Italy

ARTICLE INFO

Dataset link: https://doi.org/10.5281/zenodo.17779221

Keywords:
Extracellular vesicles
Molecular dynamics
Membranes
Elastic modulus
Cancer

ABSTRACT

Extracellular Vesicles (EVs) are increasingly employed for targeted drug delivery and advanced diagnostic assays. However, the diagnostic application of EVs so far only relied on biochemical markers as in the case of prostate cancer. Pioneering work by Whitehead and by LeClaire showed that the diagnostic power of EVs can be significantly expanded by using the mechanical properties of EV membranes for mechanophenotyping. Inspired by this idea, we computationally characterised the mechanical properties of EVs released by the prostate cancer cell line PC-3 and their healthy counterparts, the prostasomes. Our work confirms that healthy and cancer EVs exhibit different mechanical properties. However, while Whitehead and LeClaire observed a softening of the membrane in cancer EVs, our analysis reveals that the membrane of PC-3 EVs is stiffer than that of healthy prostasomes. This suggests that the diagnostic interpretation of mechanical data will have to be done on a case-by-case basis. As experimental evidence suggests that EV membranes are asymmetric, we also explored the role of numerical and compositional asymmetry starting from the PC-3 composition. Our work shows that the tilt and splay moduli of the asymmetric PC-3 membrane are the average of the moduli of the corresponding symmetric membranes. This result confirms the predictions of the elastic theory of membranes, which have been recently challenged by experimental data. Finally, our work reveals coupling effects such that the moduli of a monolayer depend not only on its composition but also on the features of the companion leaflet.

1. Introduction

Extracellular vesicles (EVs) are biological nanoparticles delimited by a lipid bilayer which encloses cytosolic proteins and RNAs.[1] They display a diverse range of sizes (30-2000 nm in diameter) and, based on their biogenesis and biophysical properties, can be classified into exosomes, microvesicles, and apoptotic bodies.[2,3] EVs are generally released by eukaryotic cells, but also by archea and bacteria. In mammals they are produced by both healthy and cancer cells, playing a crucial role in cell-free intercellular communication.[4] EVs are found in various biological fluids such as urine, blood, breast milk, saliva, pleural and amniotic fluids.[3]

EVs show a large heterogeneity in their cargo and membrane composition, which are strictly dependent on the cells of origin, as well as on the intracellular biogenetic pathway leading to their formation. In particular, the composition of the membrane influences the mechanical properties of the EVs. Such mechanical cues can be used to infer information about the status of cells from which EVs originated, e.g., healthy or cancerous.[5] Concerning cell membranes, early observations suggest that cancer cells might be softer than physiological ones, allowing them to pass small gaps in basement membranes, blood vessels, and crowded environments in the body.[6] Some specific examples are worth mentioning. Whitehead and coworkers[7] revealed that the stiffness of the EV membrane is significantly reduced in malignant bladder cells compared to physiological ones. Similarly, LeClaire et al.[8] demonstrated that the higher the malignancy of breast cancer, the lower the Young modulus of the EV membrane. Thus, the presence of a direct relationship between tumour malignancy and mechanical properties of EVs derived from these cells was suggested, which can be taken into account to characterise the existence and progression of tumours.

EVs produced by luminal cells of the prostate epithelium are defined as prostasomes.[9] They are crucial to regulate the fertilisation of spermatozoa[10] by modulating the timing of sperm cell capacitation and of the induction of the acrosome reaction, by stimulating sperm motility, and by preventing the destruction of spermatozoa by immune cells in the female reproductive tract. Prostasomes show a typical membrane composition which is essential to maintain their high stability[10]: high concentration of sphingomyelin and cholesterol, and

* Corresponding author.
E-mail address: alberto.giacomello@uniroma1.it (A. Giacomello).

https://doi.org/10.1016/j.vesic.2025.100101
Received 3 August 2025; Received in revised form 2 December 2025; Accepted 10 December 2025
Available online 26 December 2025

saturated or monounsaturated fatty acids such as palmitic acid or oleic acid, respectively. In the presence of prostate cancer, which affects more than one million men every year,[11] EVs produced by human prostate cancer cells (PC-3) change their membrane composition, similarly to what occurs to the cells they originate from Refs. 12, 13, and participate in tumour progression and in metastasis dissemination.[14] In particular, a lipidomic study[15] on the prostate cell lines RWPE-1 (non-tumourigenic), NB26 (tumourigenic), and PC-3 (metastatic) showed that EVs from tumourigenic and metastatic lines are enriched in sterol lipids, glycerophospholipids, and sphingolipids. Such changes in composition are expected to affect the mechanical properties of EVs. To verify this hypothesis, here we build and compare computational models of membranes with compositions representative of EVs derived from PC-3 cells[13] and prostasomes[16] for which a detailed composition of the two leaflets has been reported.

To date, tumour diagnosis has been based on tissue biopsy.[17] Identifying characteristic proteins in blood, called biomarkers, offers less invasive alternatives but often lacks specificity.[18] For instance, prostate-specific antigen (PSA) levels may increase not only in prostate cancer but also during infections, hyperplasia, or physical stress.[19] In this context, EVs noninvasively isolated from blood or saliva represent an emerging frontier in "liquid biopsy" which would offer an alternative to tissue biopsy.[20] Thus, the analysis of the characteristics of EVs, among which mechanical properties,[21] rather than their more analytically challenging protein components,[22] potentially offers a complementary or alternative methodology to conventional tissue biopsy for tumour diagnosis. For instance, a reduced concentration of cholesterol is considered a generic feature of cancer cells,[23] which is expected to induce some degree of softening that could be used to detect cancer.[6,24] However, as our results confirm, the picture is not as clear-cut because (i) EV composition and mechanical properties may differ significantly from those of the mother cell[13,25] in some cases leading to opposite changes in the elastic moduli,[21,26] (ii) other lipid components may affect the mechanical properties of the membrane[24] and (iii) even revert the effect of cholesterol.[27]

In this work, we focus on the mechanical properties of EV membranes derived from healthy prostasomes and PC-3 cells. We build computational models of such membranes mimicking the detailed asymmetric lipid composition of each leaflet,[13,16] in addition to control systems. As in most computational studies, we do not explicitly consider several characteristics of EV membranes which could affect the mechanical properties of actual EVs: membrane curvature, the presence membrane proteins, biomolecular corona, and cargo. The present model thus represents a first approximation of the EV complexity that will be refined in future work. Molecular Dynamics (MD) simulations were performed and mechanical properties were studied in detail. These results demonstrate that healthy and cancer EVs indeed display different mechanical signatures, but cancer EVs can be stiffer than healthy ones so that the diagnostic interpretation of the mechanical data should be made case by case. Our analysis also shows that the moduli of asymmetric membranes are intermediate compared to those of the corresponding symmetric membranes, which corroborates the predictions of the elastic theory of membranes.[28] Notably, even if our work confirms the additivity of the moduli of individual leaflets, coupling effects can be clearly observed. Given the widespread distribution of membrane asymmetry, our results aid in the clarification of a fundamental biophysical feature of membranes. From a methodological point of view, our results demonstrate the unique ability of MD simulations to build a bridge between molecular components, their dynamics, and emerging macroscopic properties of biological membranes of EVs. This computational approach complements experimental techniques, which currently exhibit strong limitations in studying both the composition and the mechanical properties of EV membranes.[29] The present approach provides a microscopic analysis of the mechanical properties of different EV membranes that could be used in the future for designing noninvasive approaches for cancer diagnostics.

2. Results

2.1. Bilayer setup

Computer models of EV membranes derived from prostate cancer cells, hereby simply named "PC-3", were produced based on lipidomics data from Skotland et al.[13] The main components of PC-3 cell membranes were identified as belonging to the families of cholesterol (CHOL), sphingomyelin (SM), phosphatidylcholines (PC), phosphatidylserines (PS), and phosphatidylethanolamines (PE). Lipidomic data normally provide a membrane-wise composition of the bilayer, but lipids belonging to these families are known to have an asymmetric distribution within the membrane. Here, we calculated the composition of individual monolayers imposing two constraints: (i) that sphingolipids are entirely located in the outer leaflet[30,31] and (ii) that phosphatidylserine and phosphatidylethanolamine are located in the inner leaflet. The base cancerous EV membrane model, named "M1", comprised asymmetric leaflet composition: in the outer leaflet 48% cholesterol (CHOL), 31% palmitoylsphingomyelin (PSM) lipids, and 21% dipalmitoylphosphatidylcholine (DPPC) lipids; in the inner leaflet 44% CHOL, 13% 1-palmitoyl-2-oleoyl-sn-glycero-3-phosphocholine (POPC) lipids, 25% 1,2-palmitoyl-oleoyl-sn-glycero-3-phosphoserine (POPS) and 18% 1-palmitoyl-2-oleoyl-sn-glycero-3-phosphoethanolamine (POPE) lipids (Table 1).

To explore the effects of different compositional and number asymmetries on the mechanical properties of the membrane,[28,32] several variants of the membrane were also generated which are summarised in Table 1. Phosphatidylserine exposed in the outer leaflet has been suggested to play a crucial role in membrane fusion and phase separation also in cancer cells and tumour-derived exosomes.[33] "M1 POPS Out" system was therefore studied, where POPS lipids were moved from the inner to the outer leaflet, replacing DPPC. "M1 -10% In" model explores the effect of asymmetry in the number of lipids, imposing a 10% reduction in all inner leaflet lipid species as compared to "M1". Two symmetric membranes were also created to ensure zero differential tension: "M1 Sym In" in which the inner leaflet composition of "M1" was replicated in both leaflets, and "M1 Sym Out" in which the outer leaflet composition was used on both sides.

Finally, the healthy prostasome membrane model "M2" was produced according to the composition reported by Arienti et al.[16]: in the outer leaflet 17% PSM lipids, 17% stearoylsphingomyelin (SSM) lipids, 6% POPC lipids, and 60% CHOL; in the inner leaflet 7% POPC, 10% 1-stearoyl-2-oleoyl-sn-glycero-3-phospho-L-serine (SOPS) lipids, 10% POPE, and 73% CHOL (Table 1).

All systems, shown in Fig. 1, were simulated with equilibrium MD simulations for several μs (see Methods for details). While systems M1 and M2 were simulated at both 303.15 K and 310.0 K, the remaining systems were simulated at 303.15 K only. The computed area per lipid (APL) shows that all membranes reached stability after 100 ns (Fig. S1). The convergence of the simulations is further confirmed by the contact analysis shown in Fig. S2.

2.2. Comparing prostasomes and PC-3 EVs

Prostate cancer PC-3 EVs (system M1) and healthy prostasomes (system M2) have a different chemical composition that suggests they may have significantly different structural and mechanical properties. The two systems were simulated at both room temperature and physiological temperature.

Fig. 2a compares the $-S_{CD}$ order parameters of system M1 at 303.15 K and 310.0 K. For the sake of graphical clarity, we only show the profiles of a sphingolipid of the outer leaflet and of a monounsaturated lipid of the inner leaflet. For both lipids, the order parameters at 310.0 K are slightly lower than those at 303.15 K as can be expected from the higher mobility of the lipids at increased temperatures. The curves at the two temperatures, however, are so

Table 1
Characteristics of the simulated systems, including composition of the leaflets, number of water molecules, total number of atoms, and dimensions of the simulation box.

System	Inner leaflet	Outer leaflet	N°H_2O	N°Atoms	Box
M1	128 CHOL 40 POPC 52 POPE 72 POPS	148 CHOL 64 DPPC 96 PSM	20276	122946	11 × 11 × 9 nm^3
M1 -10% In	115 CHOL 36 POPC 47 POPE 65 POPS	148 CHOL 64 DPPC 96 PSM	19328	117077	11 × 11 × 9 nm^3
M1 POPS Out	128 CHOL 76 POPC 88 POPE	148 CHOL 70 POPS 96 PSM	20595	124653	12 × 12 × 9 nm^3
M1 Sym Out	152 CHOL 68 POPC 100 PSM	152 CHOL 68 DPPC 100 PSM	20779	128021	11 × 11 × 9 nm^3
M1 Sym In	144 CHOL 40 POPC 56 POPE 80 POPS	144 CHOL 40 DPPC 56 POPE 80 POPS	22371	133745	12 × 12 × 9 nm^3
M2	222 CHOL 22 POPC 31 POPE 31 SOPS	180 CHOL 18 POPC 51 PSM 51 SSM	18784	112849	11 × 11 × 9 nm^3

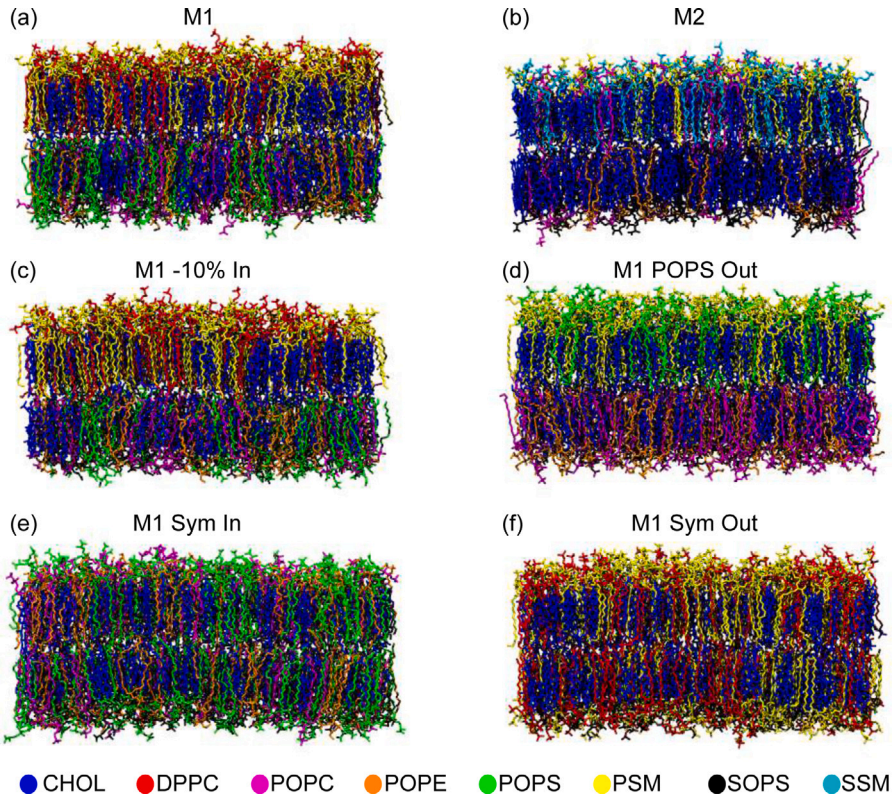

Fig. 1. Equilibrated systems where lipids are coloured by species. (a) M1, (b) M2, (c) M1 -10% In, (d) M1 POPS Out, (e) M1 Sym In, (f) M1 Sym Out.

close that the difference cannot be considered statistically significant. The same applies to the $-S_{CD}$ profiles of SSM and SOPS of the M2 system at 303.15 and 310.0 K (Fig. 2b). It can be speculated that, in this system, the cholesterol content is so high that the order parameters are only minimally affected by a modest temperature increase of 7 K. The small impact of the temperature change in these two systems is also confirmed by the fact that the area per lipid and the thickness of the two membranes remain practically unchanged at the two temperatures (Tables S1 and S2). Similar patterns are shown also by the other lipids of M1 and M2 as shown in Fig. S3.

Figs. 2c and 2d compare the order parameters of PSM and POPE of systems M1 and M2 at 303.15 K and 310.0 K, respectively. For all lipids except for the palmitic chain of PSM, the order parameters of system M2 are higher than those of M1 close to the polar heads of the lipids and lower than those of M1 in the tail region, beyond the double bond of the oleyl chain. It can be speculated that this pattern arises

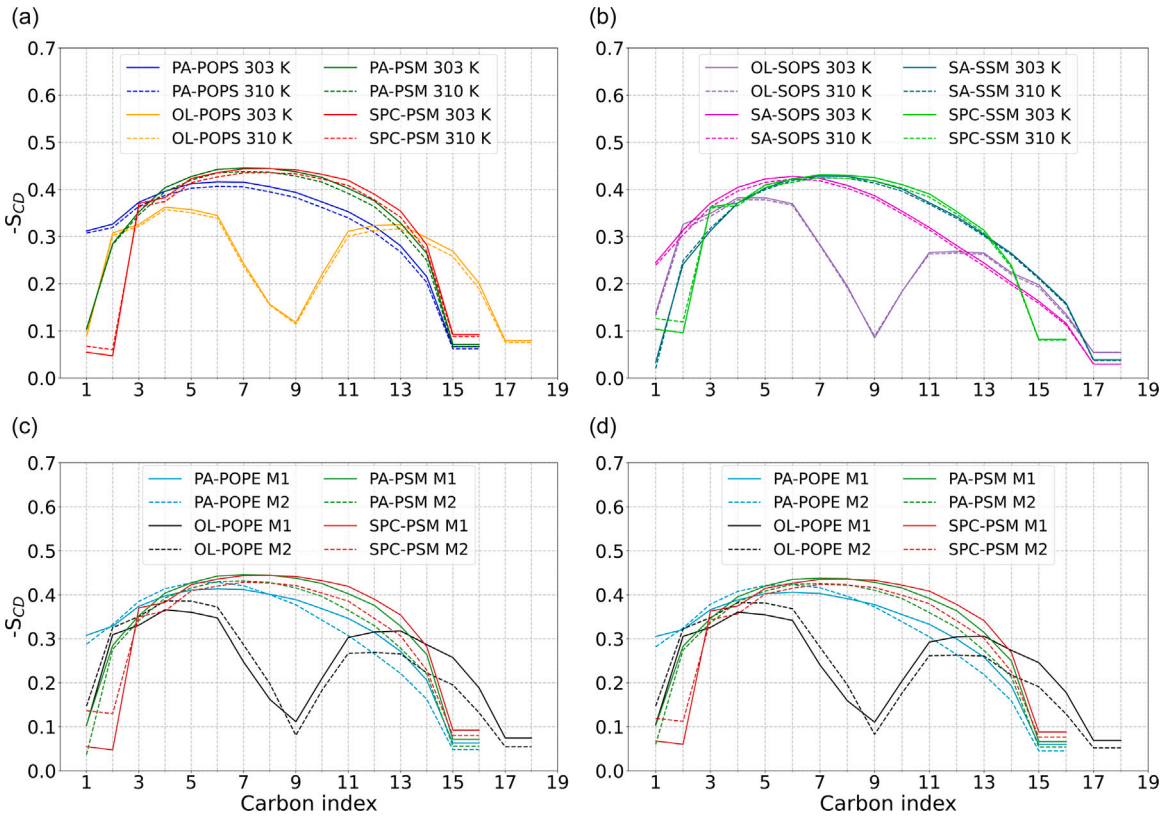

Fig. 2. Lipid order parameter profiles for some representative lipids. Panel (a) shows the profiles for POPS and PSM for system M1 at 303.15 K and 310.0 K. Panel (b) shows the profiles for SOPS and SSM for system M2 at 303.15 K and 310.0 K. Panels (c) and (d) show the profiles for POPE and PSM for systems M1 and M2 at 303.15 and 310.0 K, respectively.

from a different alignment of cholesterol and lipids in the two systems. When the cholesterol content is very high, as in M2, most of the van der Waals energy of cholesterol derives from the cholesterol/cholesterol interactions. As a result, the cholesterol molecules tend to align with each other while the alignment with the lipid molecules becomes less important. The aligned blocks of cholesterol molecules then shift close to the surface of the membrane to optimise the interaction of the hydroxyl group with water. Consequently, cholesterol improves the ordering of the lipid chains close to the polar heads while the tail regions, which are comparatively cholesterol-deprived, are left more free and therefore, more disordered. This interpretation is supported by the density profiles shown in Fig. S4. The profiles show that in system M1 cholesterol is not aligned to the polar heads of the lipids but is shifted towards the interior of the membrane to optimise the interactions with the acyl chains. By contrast, in system M2 cholesterol is more shifted towards the membrane surface, partly aligning with the polar heads. In such a way, cholesterol enhances its water exposure while spoiling its alignment with the acyl chains. The higher ordering of M2 in the polar head region is reflected by the lower area per lipid of membrane M2 as compared to M1 (Table S1).

2.2.1. Elastic properties

After comparing the structural properties of the different membranes, the mechanical properties were studied: area compressibility (K_A), splay (or bending K_C) and tilt (K_T) moduli as summarised in Fig. 3. Interesting patterns emerge from comparing the elastic properties of healthy prostasomes (M2) and cancerous PC-3 vesicles (M1). The plot in Fig. 3 reveals that system M2 at both 303.15 K and 310.0 K exhibits lower tilt and splay moduli than system M1. More insight can be gained from Tables S3 and S4 which show that, while the moduli of the inner leaflet of M2 are slightly higher than those of M1, the moduli of the outer leaflet of M2 are significantly lower than those of M1.

The results were validated by repeating the calculation of the splay moduli using the spectral analysis method introduced by Levine et al.[34] (Table S3). K_c computed with this method is equivalent to the sum of the leaflet splay moduli computed with Khelashvili's method.[32] Figure S5 shows that the moduli computed with the two methods display the same trends: M1 variants are linearly correlated and M1 is always stiffer than M2. A partial exception is system M1 -10% In, possibly due to its differential stress. Indeed, if all points are included in the analysis the linear correlation coefficient is $r = 0.86$ which increases to $r = 0.94$ if point M1 -10% In is excluded. Since the two sets of moduli are proportional, they could both be used for the comparative analyses discussed hereafter that are essentially based on the ranking of the moduli of the different systems. Quantitatively, the bending moduli computed with the spectral method are approximately 50% larger than the membrane splay moduli. This quantitative mismatch is unfortunately common when comparing absolute values of moduli obtained with different methods,[35] especially for such complex composition. Settling this issue would ultimately require experimental measurements, that are unfortunately not available for the compositions of the membranes analysed in our work.

As a further validation, we repeated our calculations with Khelashvili's method using the three alternative definitions of the lipid director and membrane normal vectors proposed in Ref. 34. The tilt and splay moduli shown in Fig. 3 were computed using director vectors pointing from the tail to the head of the lipid molecule and membrane normal vectors pointing outside the membrane. In the three alternative definitions the directors are oriented head→tail and the normal vectors point towards the interior of the membrane. Moreover, the start and end point of the director vectors were changed. In all the three alternative definitions the director vectors point to the midpoint between the terminal methyl carbons of the acyl chains. In definition A0, the director vectors start from the midpoint between the phosphorus atom

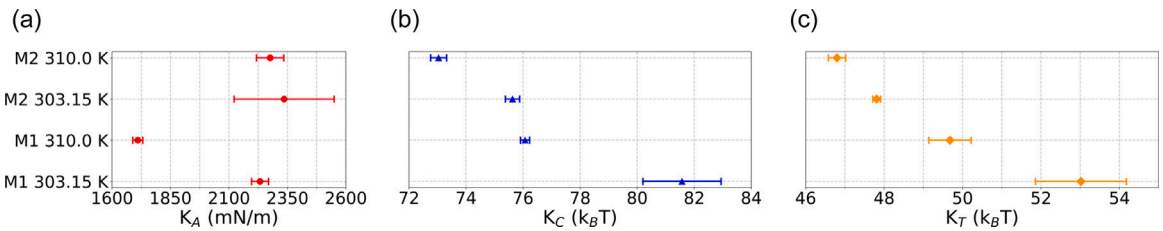

Fig. 3. Area compressibility (a), splay (b) and tilt (c) moduli for systems M1 and M2 at 303.15 K and 310.0 K.

and the glycerol C2 atom of the phospholipids (or the equivalent C2S sphingosine atom of the phospholipids). For cholesterol, the director vector links the midpoint between the O3 and C3 atoms and the C17 atom. In definition A1, the directors always originate from the phosphorus atom (or the O3 atom of cholesterol) while, in definition A2, they start from the C2 atom of phospholipids (the C2S atom of sphingolipids and the C3 atom of cholesterol). As shown in Table S6 and S7, both tilt and splay moduli were robust with respect to the definition of the director vectors, with relative changes not exceeding 10% with respect to the definitions used in the main results.

To understand the role of the different lipids on the elastic properties of the membrane it is crucial to recognise[32] that (i) the two leaflets act as springs in parallel, i.e., their moduli add up $K_{C/T} = K^{\text{out}}_{C/T} + K^{\text{in}}_{C/T}$, (ii) individual species for the leaflet tilt modulus K^l_T and lipid pairs for the leaflet splay modulus K^l_C act as springs in series such that $1/K^l_{C/T}$ are the sum of the weighted reciprocal moduli, i.e., the weighted sum of the compliances, see Eqs. (5) and (8). This means that the overall compliance of a leaflet may increase for two reasons: the modulus due to a species/pair of lipids decreases or/and its fraction increases. The "series" arrangement of lipids can thus produce unexpected effects, in our case, the softening of leaflets due to a species, cholesterol, that is generally considered to have a stiffening effect, the reason being the increase of its fraction. The direct effect of each lipid on K_T and of each pair of lipids on K_C are quantified in Fig. 4 comparing the two leaflets of M1 and M2 at 310.0 K. For both cases, the dominant contribution to the compliance comes from cholesterol which is present in large fractions: 44% (73%) and 48% (60%) for the inner and outer leaflets of M1 (M2), respectively. Although it is established that the increase of cholesterol on saturated PC lipids is typically associated with stiffer membranes,[6,24] this effect is composition-dependent, i.e., in principle depends on all other lipids as well. For example, Serral Gracià et al.[27] reported that sphingomyelin membranes become more flexible with the addition of cholesterol. Our data indeed show that cholesterol contributions to the tilt compliance $1/K^l_{T,chol}$ and the chol–chol contribution to the bending $1/K^l_{C,chol-chol}$ may have opposite signs: in the outer leaflet, they increase compliance as cholesterol content increases from M1 to M2 while the opposite applies to the inner leaflet (Fig. 4a–b). When multiplied by their fraction, however, all the contributions due to cholesterol act in the direction of increasing the compliance of both leaflets (Fig. 4c–d). Other contributions that increase the leaflets compliance going from M1 to M2 are due to the addition of SSM and POPC (outer leaflet) and SOPS (inner). Instead, the elimination of DPPC from the outer leaflet as well as the differential contributions of PSM (outer) and POPC (inner) tend to decrease the leaflets compliance in M2 in comparison with M1. The sum of these contributions results in stiffer cancerous PC-3 EV membranes (M1) as compared to the healthy counterpart (M2): $K_T = 46.80\,k_BT$ or $50.05 \cdot 10^{-20}$ J/nm^2 ($49.68\,k_BT$ or $53.13 \cdot 10^{-20}$ J/nm^2) and $K_C = 73.04\,k_BT$ or $31.24 \cdot 10^{-20}$ J ($76.07\,k_BT$ or $32.54 \cdot 10^{-20}$ J) for M2 (M1) at 310.0 K. As discussed in *Discussion and Conclusions* this unexpected result suggests that discriminating cancer advancement based on the mechanical properties of EVs is promising but the softening/stiffening effect depends on the specific compositional changes and not only on the variation in cholesterol content.

2.3. Asymmetry effects

Both healthy and cancer EVs display a highly asymmetric membrane composition that is expected to significantly affect structural and elastic properties. Fig. 5 compares the order parameters of the compositionally asymmetric system M1 with those of the corresponding symmetric systems M1 Sym In and M1 Sym Out. A comparison is also made with the system displaying number asymmetry, M1 -10% In and with system M1 POPS Out where POPS was flipped from the inner to the outer leaflet. In particular, Fig. 5a shows that the order parameters of PSM, a key lipid of the outer leaflet of M1, remain practically unchanged in M1 Sym Out that was built by duplicating the outer leaflet of M1. This suggests that the ordering of this lipid is basically unaffected by the features of the companion leaflet. Conversely, the order parameters of POPS, a typical mono-unsaturated lipid of the inner leaflet of M1, show a modest but non-negligible decrease when the lipid is part of M1 Sym In, the membrane that was generated by duplication of the inner leaflet of M1. This suggests that these order parameters can be affected by the features of the companion leaflet. Interestingly, this decrease in the order parameters of the unsaturated lipids is in agreement with a decrease in the tilt and splay moduli of the inner leaflet of M1 Sym In as compared to the inner leaflet of M1 that is compositionally identical. As illustrated in Fig. S7a–b, the behaviour of the other lipids of systems M1, M1 Sym In, and M1 Sym Out conforms to these patterns.

Fig. 5b compares the order parameters of PSM and POPS in systems M1 and M1 -10% In. It can be noted that the order parameters of PSM are practically identical in the two systems, reflecting the identical composition of the outer leaflets of the two membranes. By contrast, the order parameters of POPS are significantly lower in the system with number asymmetry. Presumably this is due to the fact that the removal of 10% of the lipids from the inner leaflet increases the area per lipid (while decreasing the membrane thickness as shown in Table S2) leaving more conformational freedom to the lipid chains. As shown in Fig. S7c–d, other lipids also exhibit similar patterns.

Fig. 5c compares systems M1 and M1 POPS Out. It can be noted that while PSM is unaffected by the presence or absence of POPS in the outer leaflet, POPS displays a moderate increase of ordering when it is moved from the inner to the outer leaflet. Presumably the ordering of POPS is a result of the replacement of the monounsaturated POPE and POPC that surrounded it in the inner leaflet, with PSM that is the main lipid partner in the outer leaflet. Finally, Fig. 5d shows the effect of the removal of POPS on the ordering of POPE, a typical unsaturated lipid of the inner leaflet. The removal of POPS causes a decrease in the order parameter profiles of POPE. This possibly reflects the ability of the polar head of POPS to establish several electrostatic and hydrogen bond interactions with its neighbours so that the flipping of this lipid to the outer leaflet results in looser interactions between the remaining lipids of the inner leaflet. As shown in Fig. S8, POPC, another important component of the inner leaflet, also behaves in the same way.

Many interesting properties emerge from the comparison of tilt and splay moduli of the whole membrane in Fig. 6c. We take as a reference the asymmetric M1 model where, as expected, the increase in temperature from 303.15 K to 310.0 K leads to a decrease in both the tilt and the splay moduli as a result of the increased mobility of lipids (Fig. 3). System M1 Sym Out was generated by duplicating the outer

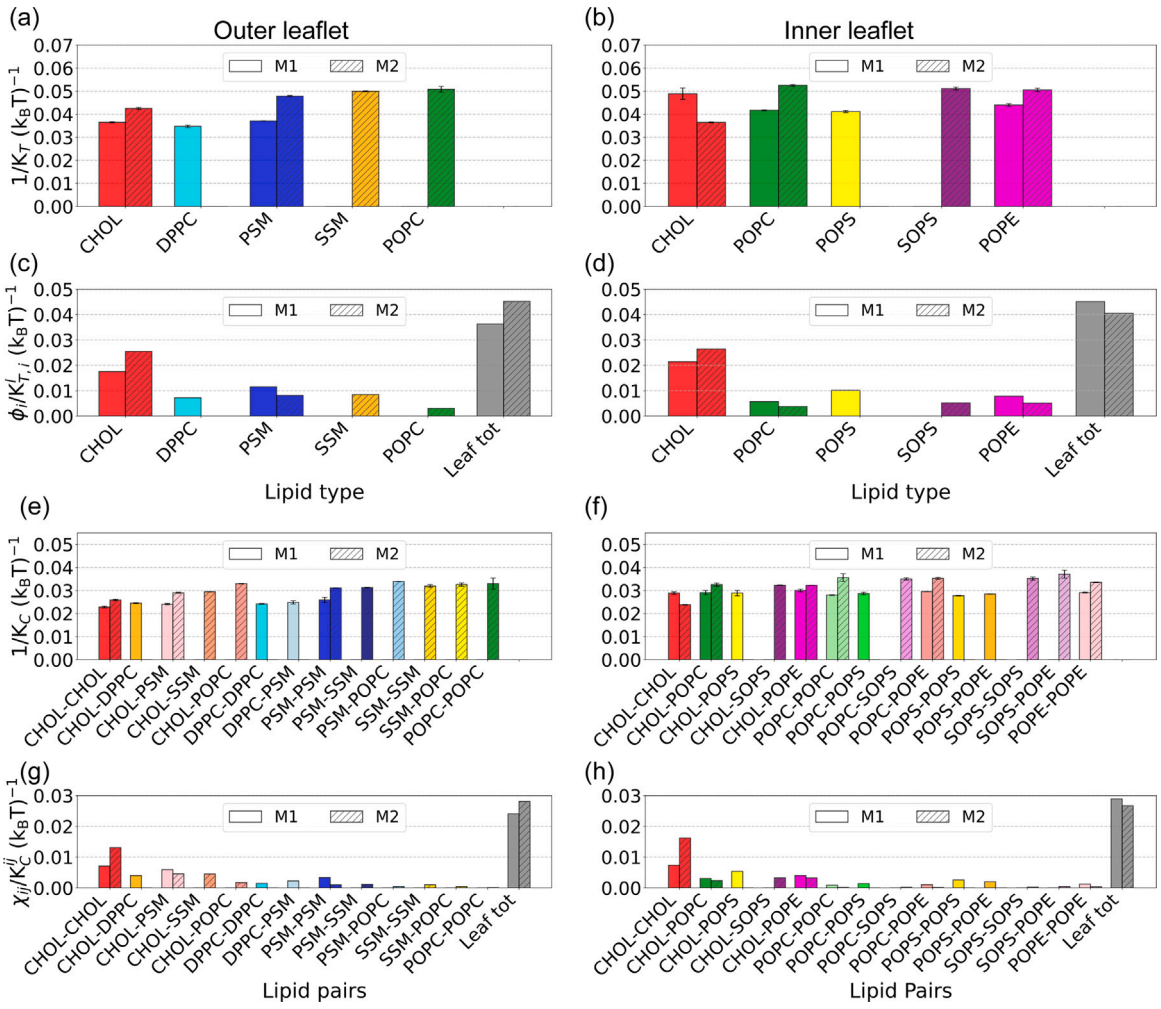

Fig. 4. Lipid contributions to the tilt (panels a–d) and splay (panels e–h) compliances of the outer (left) and inner (right) leaflets for systems M1 and M2 at 310.0 K. Panels (a) and (b) compare the tilt compliances computed for each lipid species across M1 and M2 systems. Panels (c) and (d) show the same tilt compliances weighted by the relevant lipid fractions, according to Eq. (5). Panels (e) and (f) show the splay compliances of each lipid pair. Panels (g) and (h) show the weighted splay compliances calculated using the lipid pair frequencies according to Eq. (8). The grey bars in panels (c), (d), (g), and (h) show the sum of the all tilt or splay compliances in each leaflet. The overall compliance of the two membranes are $1/K_T = 0.0201\,(k_BT)^{-1}$ and $1/K_C = 0.0131\,(k_BT)^{-1}$ for M1 and $1/K_T = 0.0212\,(k_BT)^{-1}$ and $1/K_C = 0.0137\,(k_BT)^{-1}$ for M2, showing that the cancerous EV membrane are less compliant than the healthy counterparts.

leaflet of the asymmetric membrane. Since the outer leaflet of M1 is enriched in saturated lipids, it is not surprising to discover that M1 Sym Out has higher tilt and splay moduli. In a specular way, M1 Sym In was generated by duplicating the inner leaflet of M1. Since the inner leaflet of M1 is composed of mono-unsaturated lipids, it makes sense that M1 Sym In has relatively low tilt and splay moduli. Thus, it can be observed that the moduli of the asymmetric M1 system are approximately the average of the moduli of the two corresponding symmetric membranes in agreement with the elastic theory of membranes. System M1 -10% In shows lower tilt and splay moduli compared to M1 even if the leaflets of the two membranes are populated by the same lipid species in the same proportions and the difference only consists in a decreased number of lipids in the inner leaflet. This result demonstrates that number asymmetry has a major effect on membrane elasticity.

In system M1 POPS Out, POPS was moved from the inner to the outer leaflet where it replaced DPPC. In the inner leaflet, the missing POPS was replaced by other mono-unsaturated lipids (as POPE and POPC) so that, in principle, the moduli of the inner leaflet should be almost unaffected. On the other hand, in the outer leaflet the saturated DPPC was replaced by the mono-unsaturated POPS causing a decrease in tilt and splay moduli as shown in Fig. 6.

Other interesting patterns are observed by comparing the tilt and splay moduli in the two leaflets. Again, taking as reference model M1, it can be seen that the moduli of its outer leaflet decrease when the temperature increases from 303.15 K to 310.0 K in agreement with expectations (Tables S3 and S4). It can also be seen (Fig. 6a) that even if the outer leaflet of M1 Sym Out and M1 -10% In are identical to those of M1, they exhibit significantly higher tilt and splay moduli. This suggests that the elasticity of a leaflet depends not only on its composition but also on the features of the other leaflet revealing some degree of coupling between the two leaflets. In the outer leaflet of M1 POPS Out system, at variance with M1, POPS replaces DPPC, which leads to an expected decrease in both the tilt and splay moduli. Finally, the outer leaflet of M1 Sym In has the same composition of the unsaturated inner leaflet of M1, so that this monolayer shows the lowest values of both tilt and splay moduli.

We now comment on the patterns relative to the inner leaflets of our systems (Fig. 6(b)). The moduli of the inner leaflet of M1 decrease when the temperature increases from 303.15 K to 310.0 K, presumably as a result of increased disorder (Tables S3 and S4). The inner leaflet of M1 Sym Out is equal to the saturated outer leaflet of M1, so the higher values of tilt and splay moduli are not surprising. Conversely, the inner leaflet of M1 Sym In is identical to the inner leaflet of M1 and yet M1 Sym In shows lower values of both tilt and splay modulus. This represents one more case of coupling between the two leaflets. In

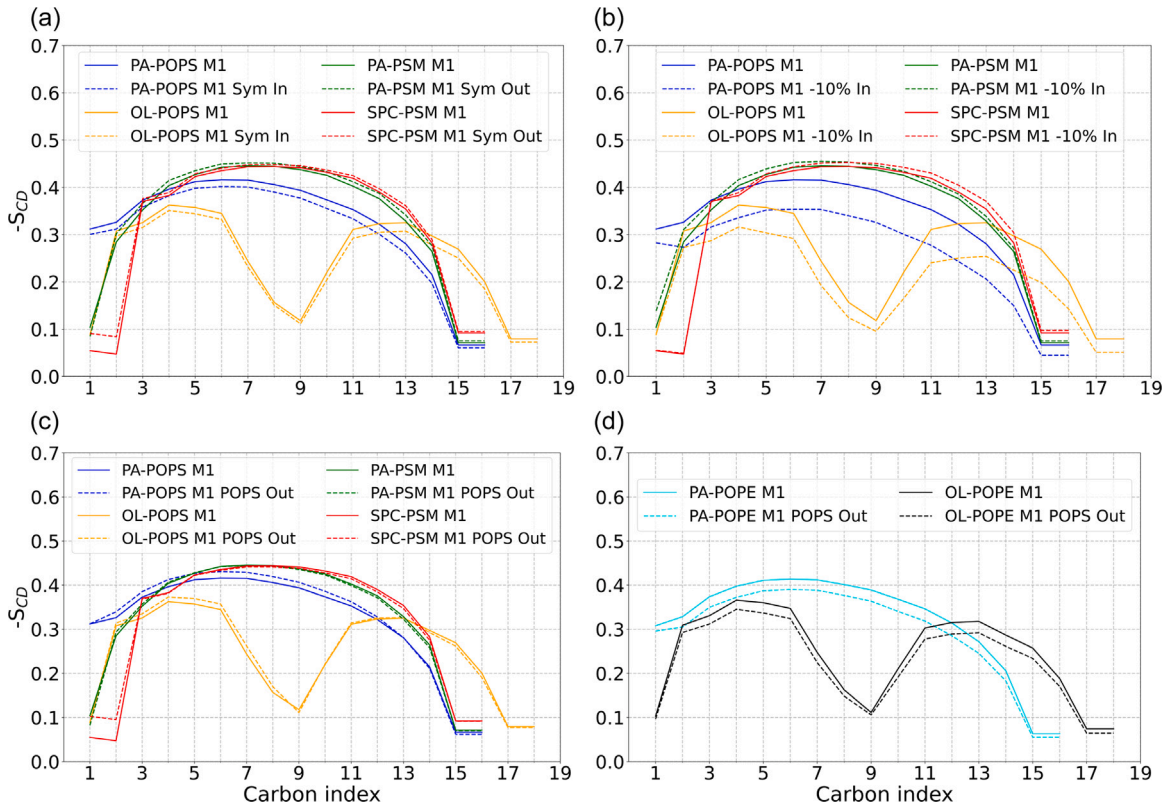

Fig. 5. Lipid order parameter profiles for some representative lipids at 303.15 K. Panel (a) shows the profiles for POPS in systems M1 and M1 Sym In and PSM in systems M1 and M1 Sym Out. Panel (b) shows the profiles for POPS and PSM for systems M1 and M1 -10% In. Panel (c) shows profiles for POPS and PSM for systems M1 and M1 POPS Out. Panel (d) shows profiles for POPE in systems M1 and M1 POPS Out.

M1 POPS Out, the inner leaflet differs from that of M1 in that POPS was replaced by POPE and POPC. The significantly lower values of tilt and splay moduli should, therefore, reflect the properties of the PS polar head. Indeed, PS is known to establish a large number of electrostatic interactions and hydrogen bonds, so its removal leads to the softening of the inner leaflet. Finally, the inner leaflet of M1 -10% In has the same lipid fractions of the inner leaflet of M1, but is deprived of 10% of its lipids. This introduces a tension that significantly decreases both elastic moduli.

It is interesting to note that despite the coupling effects, our simulations confirm the additivity of the moduli of individual leaflets. The method of Khelashvili and coworkers[32] allows us to calculate the splay moduli of individual leaflets of the symmetric systems M1 Sym Out and M1 Sym In (46.10 and 33.44 k_BT on average or 19.29 and $13.99 \cdot 10^{-20}$ J, Table S3). The sum of these two values leads to an estimated value of 79.54 k_BT ($33.27 \cdot 10^{-20}$ J) for the asymmetric M1 system at 303.15 K which is consistent with $K_C = 81.58\ k_BT$ ($34.12 \cdot 10^{-20}$ J) derived from the simulation at 303.15 K. Following a similar argument, tilt moduli also show additivity such that the tilt modulus of M1 at 303.15 K predicted from the simulations of the symmetric systems ($K_T = 51.5\ k_BT$ or $53.85 \cdot 10^{-20}$ J/nm^2), is in substantial agreement with $K_T = 53\ k_BT$ or $55.42 \cdot 10^{-20}$ J/nm^2 that was attained from the simulation of M1.

It should be noted that our protocol does not allow for a separate calculation of the area compressibility moduli for the two leaflets. However, since the two leaflets can be modelled as two springs in parallel, the moduli of the individual leaflets of the symmetrical membranes can be calculated by halving the value of K_A of the entire membrane. For M1 Sym Out and M1 Sym In, this leads to 1680.5 and 576 mN/m, respectively (see Table S5). If these two values are summed, we get a prediction of the K_A value of the asymmetric M1 system at 303.15 K: 2256.5 mN/m. This estimate is fully consistent with the value of K_A for the M1 system computed from the simulation at 303.15 K. Therefore, our calculations also confirm the additivity of the area compressibility moduli.

3. Discussion and conclusions

Extracellular vesicles are raising significant interest for their potential biomedical applications, both in the field of targeted drug delivery and of minimally invasive diagnostic assays.[36] However, the clinical application of EVs is still limited by problems of isolation and purification.[37] Indeed, due to the existence of a multitude of classes of biological nanoparticles,[38] the classification of EVs based on biochemical markers fails to provide an unambiguous signature that would be necessary for purification, characterisation, and engineering. The current trend, therefore, is to characterise EVs in terms of mesoscale signatures like their mechanical properties, that can be measured, for example, by Atomic Force Microscopy (AFM),[21,39,40] 3D-AFM,[26] and non-contact microfluidics.[41] In addition, the elasticity of engineered drug delivery nanoparticles influences their blood circulation, phagocytosis, endocytosis, and targeting.[42]

Mechanical properties are important not only for purification but also for diagnostics. Diagnostic assays, however, typically employ only biochemical markers as membrane proteins. Whitehead et al.[7] showed that the use of mechanical properties could significantly expand the power of diagnostic assays. In their study, Whitehead et al. compared EVs released by healthy and cancer urothelial cells that were undistinguishable on the basis of all known biochemical markers and could only be discriminated considering their mechanical properties. In particular, they observed that EVs released by cells derived from bladder carcinoma tend to be softer than those produced by healthy urothelial cells. These results are in agreement with the findings of LeClaire[8] showing a progressive softening of the EV membrane as breast-derived cells progress towards malignancy and invasivity. In

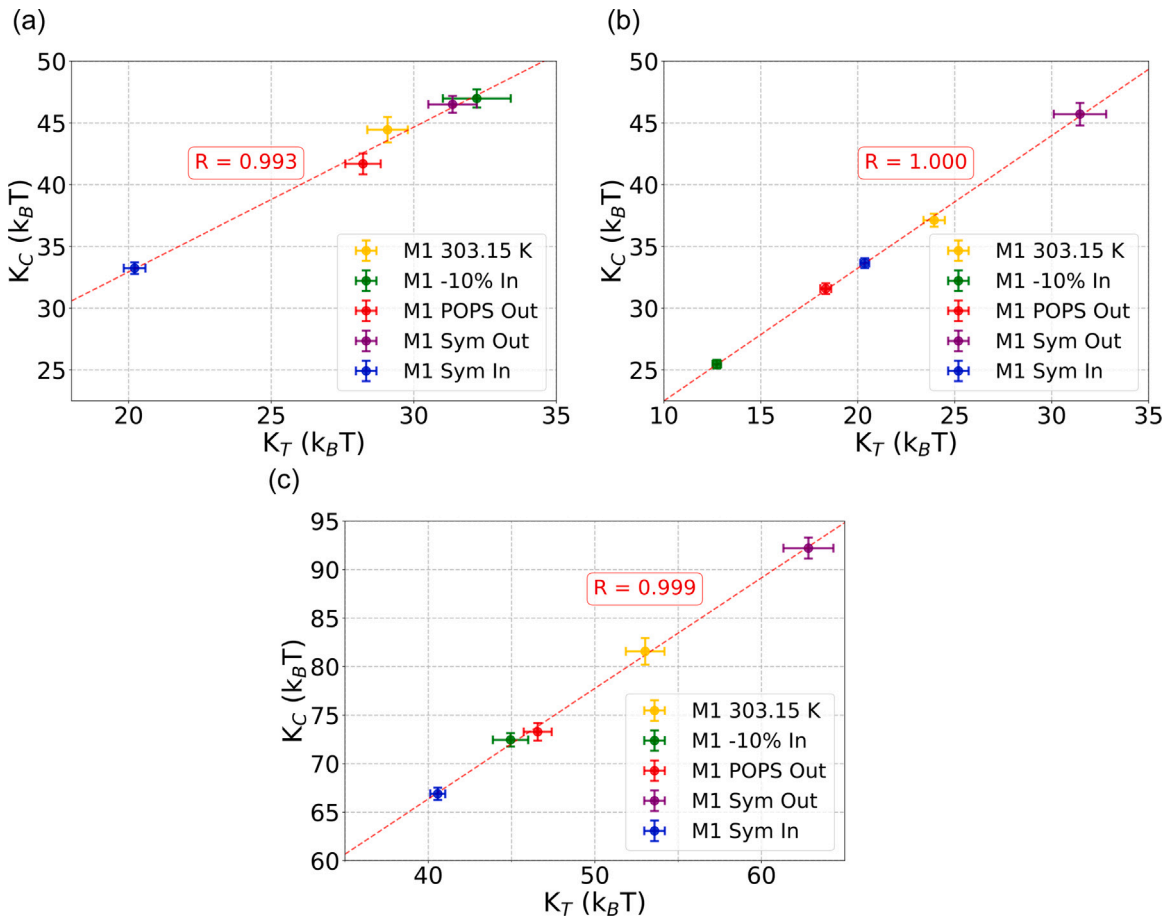

Fig. 6. Coupling plots between (a) tilt and splay for the outer leaflet, (b) tilt and splay for the inner leaflet and (c) tilt and splay for the whole membrane.

this work, we focused on the EVs released by the prostate cancer cell line PC-3, together with their healthy counterpart, the prostasomes. In agreement with Whitehead[7] and LeClaire,[8] we found different values of the tilt and splay moduli, but the cancerous PC-3 vesicles turned out to be stiffer than the healthy prostasomes. Our detailed analysis of the contributions of each lipid type to the overall elastic moduli of the membrane underscores a complex interplay among lipid types, with the reduction in cholesterol content providing the dominant contribution to the stiffening of PC-3 cancerous EV membranes (Fig. 4), similar to the role that it has in sphingomyelin membranes.[27] These results suggest that, in each type of cancer, the EV membrane can become more[21,26] or less[7,8] rigid than that of healthy vesicles, so that the diagnostic interpretation of mechanical properties will have to be made case-by-case. This nuanced scenario underscores the need for systematic experimental measurements of the mechanical properties of EVs at different cancer stages to confirm the present predictions and, more generally, to identify diagnostically relevant trends. Additionally, biofluids usually contain only a minor fraction of EVs, which poses practical challenges to the use of the proposed mechanophenotyping strategy. Nonetheless, this approach has been demonstrated in EVs isolated from blood and bone marrow samples,[21] can be implemented using high-throughput techniques,[40,43] and could serve as the basis for multimodal EV screening.[44]

Many of the results of this work originate in the asymmetric composition of EV membranes and therefore go much beyond the scope of prostate cancer diagnostics. Membrane asymmetry, that has been known to the biophysical community since the early 1970s,[45] can be considered as an almost universal property of biological membranes, with conservation in all kingdoms of nature. However, the study of asymmetry was severely limited by the difficulty in producing model membranes with a simplified composition. Recently, this problem has been solved with the advent of the phase transfer technique[46] that allows the assembly of lipid bilayers with tailored composition. Using this approach, the bending modulus of an asymmetric DOPC/POPC membrane was measured showing that the asymmetric membrane is much more rigid than both corresponding symmetric bilayers.[46] These results, however, have been questioned on theoretical grounds by Hossein and Deserno[28] who suggested that the creation of compositionally asymmetric membranes may induce an accidental differential stress so that the membrane looks stiffer than it actually is. According to this interpretation, in the mentioned experiment, it is number asymmetry rather than composition asymmetry that affects the rigidity of a membrane.

In agreement with the elastic theory of membranes,[28] our simulations showed that the tilt and splay moduli of the asymmetric M1 membrane are the average of the moduli of the symmetric membranes built duplicating the inner and outer leaflet of M1. Our simulations, performed with state-of-the-art atomistic force field and membranes with complex and realistic compositions, thus strengthen Deserno's own validation, which was based on coarse-grained MARTINI simulations of simple model membranes.[28] However, while in Deserno's work the bending modulus increased with increasing numerical asymmetry, in our case a numerical asymmetry of 10% results in a less rigid membrane. This difference is possibly justified by the fact that our compositions are much more complex than Deserno's and in our systems there could be some interplay between numerical and compositional asymmetry.

Finally, our work shows several examples of coupling between the two leaflets, whereby the tilt and splay moduli of a leaflet depend not only on the chemical composition of that leaflet, but also on the

Table 2
Duration of each MD simulation and reference point after which the systems reached the convergence, which was monitored using the evolution of the area per lipid and lipid–lipid contacts.

System	Temperature	Time	Convergence
M1 303.15 K	303.15 K	8.5 μs	5.0 μs
M1 310.0 K	310.0 K	4.0 μs	1.5 μs
M1 -10% In	303.15 K	5.5 μs	2.5 μs
M1 POPS Out	303.15 K	8.5 μs	3.5 μs
M1 Sym Out	303.15 K	8.5 μs	3.5 μs
M1 Sym In	303.15 K	8.5 μs	1.0 μs
M2 303.15 K	303.15 K	3.0 μs	0.5 μs
M2 310.0 K	310.0 K	3.0 μs	0.5 μs

features of the companion one. Although the molecular basis of this behaviour is still a work in progress, it is noteworthy that, in agreement with elastic theory, membrane asymmetry does not undermine the additivity of the moduli, but slightly changes the moduli of individual leaflets based on the interactions with the partner monolayer.

In short sum, our computational work makes a case for the application of the mechanical properties of EV membranes to diagnostic, e.g., in the case of prostate cancer, showing an unexpected stiffening behaviour due to nontrivial compositional changes. We also discuss some implications of membrane asymmetry, showing that, while the additivity of the moduli is preserved, interesting coupling effects can be detected. Additional research efforts, including more complex computer models of EV membranes and experimental measurements of their elastic properties, will be needed to confirm the reported trends and advance EV-based mechanophenotyping.

Methods

MD simulations

All membranes were generated using the CHARMM-GUI Membrane Builder[47,48] and solvated with a 0.15 M NaCl in TIP3P water[49] solution. MD simulations were run with GROMACS 2023.3[50] using the CHARMM36m force field.[51,52] After a minimisation and equilibration as in the standard six-step CHARMM-GUI protocol,[53] each system was simulated for several μs in the NPT ensemble. The details of different systems are provided in Table 2. The pressure was kept at 1 atm by the Parrinello–Rahman barostat[54–56] with a damping coefficient of 0.5 ps and an optimal compressibility of 4.5×10^{-5} bar^{-1} for water. The temperature was maintained at 303.15 or 310.0 K using the Nosé–Hoover thermostat[57,58] with a damping coefficient of 1 ps^{-1}. Electrostatic interactions were taken into account by implementing a fast and smooth Particle-Mesh Ewald algorithm[59] with a 12 Å distance for the Coulomb cutoff. The integration time step was 2 fs.

Calculation of membrane properties

The membrane thickness (h) of each membrane was computed using the peaks of the phosphorus mass density profiles averaged over the whole trajectories.

We quantified membrane ordering using the acyl chain order parameters $-S_{CD}$[60]:

$$S_{CD} = \frac{\langle 3\cos^2(\beta) - 1 \rangle}{2} \tag{1}$$

where β is the angle formed by the C–H bond vector with the bilayer normal, and the brackets $\langle \cdots \rangle$ represent an average over all lipids of the same species and all time frames sampled during the simulation.

The area per lipid (APL) was computed as:

$$\text{APL} = \frac{\text{A}_{\text{Lateral}}}{\text{N}_{\text{Lipid}}} \tag{2}$$

where $\text{A}_{\text{Lateral}}$ is the membrane lateral area and N_{Lipid} is the number of lipids in the leaflet.

Tilt modulus calculations

The tilt modulus (K_T) was computed as described by Doktorova et al.[32] The calculation starts with the tilt angle distribution that is attained by substituting the energy for tilt deformation in the Boltzmann distribution:

$$P(\theta) = C_t \sin(\theta) \exp\left(-\frac{1}{4k_B T} K_T A_l \theta^2\right) \tag{3}$$

where $P(\theta)$ is the probability distribution of tilt angles θ, $\sin(\theta)$ is the degeneracy term, A_l is the area per lipid, k_B is the Boltzmann constant, and C_t is a normalisation constant. For small angles, $\tan^2\theta \approx \theta^2$. The potential of mean force (PMF) is then:

$$\text{PMF}(\theta) = -4k_B T \ln\left(\frac{P(\theta)}{\sin\theta}\right) = K_T^l \theta^2 + C_t' \tag{4}$$

with $K_T^l = K_T A_l$ denoting the tilt modulus per lipid. The tilt modulus is obtained by fitting the PMF with a quadratic function. For a leaflet composed of different lipid species, K_T^l is computed by considering the different lipids as springs in series:

$$\frac{1}{K_T^l} = \sum_i \frac{\phi_i}{K_{T,i}^l} \tag{5}$$

where $\phi_i = N_i / N_{\text{tot}}$, N_i, and $K_{T,i}^l$ are the fraction, number of lipids, and tilt modulus for species i, respectively. K_T of the entire lipid bilayer is approximated by summing the leaflet moduli, treating the leaflets as parallel springs. Lipid director vectors are computed from the centres of mass of tail and headgroups atoms. To check the dependence on this definition, we repeated the K_T calculations for M1 and M2 at 310.0 K using the definitions given in previous work[6,34]; results are reported in Table S6. Tilt angles were sampled across trajectories and PMFs were fitted in suitable intervals to determine K_T values.

Splay modulus calculations

The splay modulus (K_C) was computed using the lipid splay approach, where the splay angle α is defined as the angle between director vectors of neighbouring lipids.[61,62] The robustness of the splay moduli calculation with respect to the definition of the director vector was also tested using the alternative definitions of this vector[6,34] for M1 and M2 at 310 K (Table S7). Assuming independent splay deformations, the Boltzmann distribution describes the probability of a given angle α:

$$P(\alpha) = C_b \sin(\alpha) \exp\left(-\frac{K_C A_l \alpha^2}{2k_B T}\right) \tag{6}$$

where A_l is the area per lipid, $\sin(\alpha)$ is the degeneracy of the angles, k_B is the Boltzmann constant, and C_b is a normalisation constant. The associated PMF is:

$$\text{PMF}(\alpha) = -2k_B T \ln\left(\frac{P(\alpha)}{\sin\alpha}\right) = K_C^l \alpha^2 + C_b' \tag{7}$$

with $K_C^l = K_C A_l$. K_C is obtained by fitting this PMF with a quadratic function. In multicomponent systems, the PMF is computed separately for each lipid pair and the leaflet splay modulus is obtained via the weighted average:

$$\frac{1}{K_C^l} = \sum_{i,j} \frac{\chi_{ij}}{K_C^{ij}} \tag{8}$$

where the lipid pair fraction $\chi_{ij} = \phi_{ij} / \phi_{\text{tot}}$ is calculated based on the number of sampled lipid pairs ϕ_{ij} of species i and j, ϕ_{tot} is the total number of pairs, and K_C^{ij} is the corresponding splay modulus. The bilayer splay modulus is calculated by summing the moduli of the two leaflets. Splay angles were obtained by sampling pairs of lipid director vectors within a 1 nm cutoff. Angle distributions were used to compute the PMFs, from which K_C^{ij} values were extracted via quadratic fitting over various intervals.

Splay modulus calculations (spectral method)

In order to validate the values of the membrane moduli computed using Khelashvili's method above, the calculation was repeated using the spectral method introduced by Levine et al.[34] The key quantity is the unit director vector $\mathbf{n}_j^\alpha$ of lipid j belonging to leaflet $\alpha \in \{1,2\}$ for the outer and inner monolayers, respectively. The unit vector originates in the midpoint between the P atom and the C2 atom of the glycerol unit and points towards the midpoint between the two terminal methyl carbons of the acyl chains. The director vector is projected on the xy plane and Fast Fourier Transformed yielding a matrix of $\mathbf{n}_\mathbf{q}^\alpha$ vectors for each monolayer (where $\mathbf{q}$ is the 2D Fourier wavevector). We used a continuous approximation of the Fast Fourier Transform multiplying it by $dxdy$ where, in our square grid, $dx = dy = L/N_c$, L is the box length and N_c the number of cells in which each dimension is discretised. The Fast Fourier Transform was then normalised dividing by the box length following Ref. 63. The algorithm then requires the calculation of a related bilayer quantity $\hat{\mathbf{n}}_\mathbf{q} = [\mathbf{n}_\mathbf{q}^{(1)} - \mathbf{n}_\mathbf{q}^{(2)}]/2$ that is decomposed in a longitudinal component $\hat{\mathbf{n}}_\mathbf{q}^\parallel = [\mathbf{q} \cdot \hat{\mathbf{n}}_\mathbf{q}]/q$ and a transverse component $\hat{\mathbf{n}}_\mathbf{q}^\perp = [\mathbf{q} \times \hat{\mathbf{n}}_\mathbf{q}] \cdot \hat{z}/q$. The averaged squared modulus of these quantities finally allows the comparison with the theoretical predictions:

$$\langle |\hat{\mathbf{n}}_\mathbf{q}^\parallel|^2 \rangle = \frac{k_B T}{K_C q^2} \tag{9}$$

$$\langle |\hat{\mathbf{n}}_\mathbf{q}^\perp|^2 \rangle = \frac{k_B T}{K_T + K_{Tw} q^2} \tag{10}$$

where K_C, K_T, and K_{Tw} are the bending, tilt and twist moduli that can be computed as fitting parameters. The bending modulus is equivalent to the bilayer splay modulus computed with Khelashvili's method. In contrast, as discussed by Doktorova et al.,[32] the tilt modulus derived from spectral analysis methods such as Levine's, is not directly comparable to the tilt modulus computed with real space fluctuation methods like Khelashvili's. Indeed the tilt modulus derived from spectral methods is just an additive component and thus it is smaller than the tilt modulus from real space fluctuation methods. The difference between these two quantities is associated to losses in orientational entropy of the lipid chains, but its entity is still debated. For this reason, no comparison was made between the tilt moduli computed using Levine's and Khelashvili's methods.

The implementation of our codes for the calculation of bending/splay moduli with the methods of Khelashvili and Brown was benchmarked using a simple membrane composed by 648 DOPC molecules at 298 K which was also used in the original Refs. 32, 34. Details on the simulation protocol can be found in Ref. 34 while the results of the test are displayed in Table S8.

Figure S6 shows the plot of $q^2\langle |\mathbf{n}_\mathbf{q}^\parallel|^2 \rangle$ as a function of the modulus q of the wave vector for systems M1 and M2 at 310.0 K. As shown by Eq. (9), the theory predicts that for small values of q this quantity should tend to the constant value $k_B T/K_C$. Indeed the curves shown in Fig S6 are almost flat for $q < 1.25$ nm^{-1} or, equivalently, for a length scale >5.0 nm. This means that the spectral method is valid for membranes with a box length of 11–12 nm as those analysed in the present work.

Area compressibility modulus calculations

The area compressibility modulus (K_A) was calculated using two methods.[64] In the first one, assuming small deformations and applying the equipartition theorem ($\langle E \rangle = \frac{1}{2} k_B T$), K_A is obtained from the average and variance of the lateral area of the simulation box:

$$K_A = \frac{a_0}{\langle (a - a_0)^2 \rangle} k_B T \tag{11}$$

where a_0 is the average area and a the instantaneous area per frame. In the second method, the distribution of relative area fluctuations $\Delta a/a_0$ follows a Boltzmann form, leading to the potential of mean force:

$$\mathrm{PMF}\left(\frac{\Delta a}{a_0}\right) = -\frac{2k_B T}{a_0} \ln P\left(\frac{\Delta a}{a_0}\right) = K_A \left(\frac{\Delta a}{a_0}\right)^2 + C' \tag{12}$$

where C' is a constant. K_A is extracted by fitting the PMF with a quadratic function. Thus, following the first method, K_A was computed from area variance; in the second, from fitting the PMF derived from the distribution of $\Delta a/a_0$ values sampled over time. The two methods validated each other producing results in excellent agreement.

Statistics and reproducibility

A block analysis was applied[65,66] to characterise the variability of the computational quantities reported in this work. Each simulation was split in a number N_B of blocks, each of 500 ns; the observables of interest ($\overline{X}_B$) in the various blocks could be considered as uncorrelated. From that, it was possible to compute the variance of the mean of any observable:

$$\sigma^2((\overline{X})_B) = \frac{1}{N_B(N_B - 1)} \sum_{i=1}^{N_B} ((\overline{X})_B - \langle (\overline{X})_B \rangle)^2 \tag{13}$$

CRediT authorship contribution statement

Carlo Guardiani: Writing – review & editing, Writing – original draft, Supervision, Methodology, Investigation, Formal analysis. **Matteo Riboli:** Writing – original draft, Visualization, Investigation, Formal analysis. **Flavio Costa:** Writing – original draft, Supervision, Investigation. **Massimiliano Bruno:** Investigation, Formal analysis, Data curation. **Giulia Rossi:** Writing – review & editing, Project administration, Methodology, Conceptualization. **Alberto Giacomello:** Writing – review & editing, Supervision, Resources, Project administration, Funding acquisition, Conceptualization.

Declaration of competing interest

The authors declare that they have no known competing financial interests or personal relationships that could have appeared to influence the work reported in this paper.

Acknowledgements

CG thanks Paolo Gualtieri for useful discussion on FFT. The authors acknowledge EuroHPC for awarding them access to MareNostrum5 at Barcelona Supercomputing Center, Spain. F.C. and A.G. acknowledge the financial support of the Italian Ministry of Education, University, and Research (MIUR) through the "Framework per l'Attrazione e il Rafforzamento delle Eccellenze per la Ricerca in Italia (FARE)" scheme, grant SERENA n. R18XYKRW7J. We acknowledge financial support under the National Recovery and Resilience Plan (NRRP), Mission 4, Component 2, Investment 1.1, Call for tender No. 1409 published on 14.9.2022 by the Italian Ministry of University and Research (MUR), funded by the European Union – NextGenerationEU – Project Title "The virtual EV (v-EV): A digital twin of extracellular vesicles for health and food" –CUP B53D23027530001 - Grant Assignment Decree No. 1389 adopted on 01/09/2023 by the Italian Ministry of University and Research (MUR). All authors approved the final version of the manuscript.

Appendix A. Supplementary data

The following files are available free of charge.

- Structural and Mechanical parameters, APL profiles, contacts analysis, acyl chain order parameter profiles, density profiles, and power spectra.

Supplementary material related to this article can be found online at https://doi.org/10.1016/j.vesic.2025.100101.

Data availability

The data underlying this study are available in the published article and its Supporting Information. The MD trajectories, an example of the input file, and the topology files are openly available in ZENODO, https://doi.org/10.5281/zenodo.17779221.

References

1. Welsh JA, Goberdhan DC, O'Driscoll L, et al. Minimal information for studies of extracellular vesicles (misev2023): From basic to advanced approaches. *J Extracell Vesicles*. 2024;13(2):e12404.
2. Akers JC, Gonda D, Kim R, Carter BS, Chen CC. Biogenesis of extracellular vesicles (ev): exosomes, microvesicles, retrovirus-like vesicles, and apoptotic bodies. *J Neurooncol*. 2013;113:1–11.
3. Stavrou A, Ortiz A. Extracellular vesicles: a novel tool in nanomedicine and cancer treatment. *Cancers*. 2022;14(18):4450.
4. Tkach M, Théry C. Communication by extracellular vesicles: where we are and where we need to go. *Cell*. 2016;164(6):1226–1232.
5. Yáñez Mó M, Siljander PR-M, Andreu Z, et al. Biological properties of extracellular vesicles and their physiological functions. *J Extracell Vesicles*. 2015;4(1):27066.
6. Nguyen HL, Man VH, Li MS, Derreumaux P, Wang J, Nguyen PH. Elastic moduli of normal and cancer cell membranes revealed by molecular dynamics simulations. *Phys Chem Chem Phys*. 2022;24(10):6225–6237.
7. Whitehead B, Wu L, Hvam ML, et al. Tumour exosomes display differential mechanical and complement activation properties dependent on malignant state: implications in endothelial leakiness. *J Extracell Vesicles*. 2015;4(1):29685.
8. LeClaire M, Wohlschlegel JA, Chang H, et al. Nanoscale extracellular vesicles carry the mechanobiology signatures of breast cancer cells. *ACS Appl Nano Mater*. 2021;4(9):9876–9885.
9. Vickram A, Samad HA, Latheef SK, et al. Human prostasomes an extracellular vesicle–biomarkers for male infertility and prostrate cancer: The journey from identification to current knowledge. *Int J Biiol Macromol*. 2020;146:946–958.
10. Aalberts M, Stout T, Stoorvogel W, et al. Prostasomes: extracellular vesicles from the prostate. *Reproduction*. 2014;147(1):R1–14.
11. Bray F, Laversanne M, Sung H, et al. Global cancer statistics 2022: Globocan estimates of incidence and mortality worldwide for 36 cancers in 185 countries. *CA: Cancer J Clin*. 2024;74(3):229–263.
12. Róg T, Orłowski A, Llorente A, et al. Interdigitation of long-chain sphingomyelin induces coupling of membrane leaflets in a cholesterol dependent manner. *Biochim et Biophys Acta (BBA)-Biomembranes*. 2016;1858(2):281–288.
13. Skotland T, Sagini K, Sandvig K, Llorente A. An emerging focus on lipids in extracellular vesicles. *Adv Drug Deliv Rev*. 2020;159:308–321.
14. Fonseka P, Liem M, Ozcitti C, Adda CG, Ang C-S, Mathivanan S. Exosomes from n-myc amplified neuroblastoma cells induce migration and confer chemoresistance to non-n-myc amplified cells: Implications of intra-tumour heterogeneity. *J Extracell Vesicles*. 2019;8(1):1597614.
15. Brzozowski JS, Jankowski H, Bond DR, et al. Lipidomic profiling of extracellular vesicles derived from prostate and prostate cancer cell lines. *Lipids Health Dis*. 2018;17(1):211.
16. Arienti G, Carlini E, Polci A, Cosmi E, Palmerini C. Fatty acid pattern of human prostasome lipid. *Arch Biochem Biophys*. 1998;358(2):391–395.
17. Vaidyanathan R, Soon RH, Zhang P, Jiang K, Lim CT. Cancer diagnosis: from tumor to liquid biopsy and beyond. *Lab A Chip*. 2019;19(1):11–34.
18. Basil CF, Zhao Y, Zavaglia K, et al. Common cancer biomarkers. *Cancer Res*. 2006;66(6):2953–2961.
19. Balk SP, Ko Y-J, Bubley GJ. Biology of prostate-specific antigen. *J Clin Oncol*. 2003;21(2):383–391.
20. Ma L, Guo H, Zhao Y, et al. Liquid biopsy in cancer current: status, challenges and future prospects. *Signal Transduct Target Ther*. 2024;9(1):336.
21. Feng Y, Liu M, Li X, Li M, Xing X, Liu L. Nanomechanical signatures of extracellular vesicles from hematologic cancer patients unraveled by atomic force microscopy for liquid biopsy. *Nano Lett*. 2023;23(4):1591–1599.
22. Coumans FA, Brisson AR, Buzas EI, et al. Methodological guidelines to study extracellular vesicles. *Circ Res*. 2017;120(10):1632–1648.
23. Szlasa W, Zendran I, Zalesińska A, Tarek M, Kulbacka J. Lipid composition of the cancer cell membrane. *J Bioenerg Biomembr*. 2020;52(5):321–342.
24. Pöhnl M, Trollmann MF, Böckmann RA. Nonuniversal impact of cholesterol on membranes mobility. *Curvature Sens Elast Nat Commun*. 2023;14(1):8038.
25. Ghadami S, Dellinger K. The lipid composition of extracellular vesicles: applications in diagnostics and therapeutic delivery. *Front Mol Biosci*. 2023;10:1198044.
26. Yurtsever A, Yoshida T, Behjat AB, Araki Y, Hanayama R, Fukuma T. Structural and mechanical characteristics of exosomes from osteosarcoma cells explored by 3d-atomic force microscopy. *Nanoscale*. 2021;13(13):6661–6677.
27. Serral Gracià R, Bezlyepkina N, Knorr RL, Lipowsky R, Dimova R. Effect of cholesterol on the rigidity of saturated and unsaturated membranes: fluctuation and electrodeformation analysis of giant vesicles. *Soft Matter*. 2010;6(7):1472–1482.
28. Hossein A, Deserno M. Spontaneous curvature, differential stress, and bending modulus of asymmetric lipid membranes. *Biophys J*. 2020;118:624–642.
29. Piontek MC, Lira RB, Roos WH. Active probing of the mechanical properties of biological and synthetic vesicles. *Biochim et Biophys Acta (BBA)-General Subj*. 2021;1865(4):129486.
30. Hallal S, Tűzesi Á, Grau GE, Buckland ME, Alexander KL. Understanding the extracellular vesicle surface for clinical molecular biology. *J Extracell Vesicles*. 2022;11(10):e12260.
31. Russell AE, Sneider A, Witwer KW, et al. Biological membranes in ev biogenesis, stability, uptake, and cargo transfer: an isev position paper arising from the isev membranes and evs workshop. *J Extracell Vesicles*. 2019;8(1):1684862.
32. Doktorova M, Harries D, Khelashvili G. Determination of bending rigidity and tilt modulus of lipid membranes from real-space fluctuation analysis of molecular dynamics simulations. *Phys Chem Chem Phys*. 2017;19(25):16806–16818.
33. Perez GI, Bernard MP, Vocelle D, et al. Phosphatidylserine-exposing annexin a1-positive extracellular vesicles: potential cancer biomarkers. *Vaccines*. 2023;11(3):639.
34. Levine ZA, Venavle RM, Watson MC, et al. Determination of biomembrane bending moduli in fully atomistic simulation. *J Am Chem Soc*. 2014;136:13582–13585.
35. Hu M, Diggins P, Deserno M. Determining the bending modulus of a lipid membrane by simulating buckling. *J Chem Phys*. 2013;138(21).
36. Stawarska A, Bamburowicz-Klimkowska M, Runden-Pran E, et al. Extracellular vesicles as next-generation diagnostics and advanced therapy medicinal products. *Int J Mol Sci*. 2024;25:6533.
37. Gori A, Romanato A, Bergamaschi G, et al. Membrane-binding peptides for extracellular vesicles on-chip analysis. *J Extracell Vesicles*. 2020;9:1751428.
38. Busatto S, Presta M, Zendrini A, et al. The nanostructured secretome. *Biomater Sci*. 2020;8:39–63.
39. Parisse P, Rago I, Ulloa Severino L, et al. Atomic force microscopy analysis of extracellular vesicles. *Eur Biophys J*. 2017;46(8):813–820.
40. LeClaire M, Gimzewski J, Sharma S. A review of the biomechanical properties of single extracellular vesicles. *Nano Sel*. 2021;2(1):1–15.
41. Jeong MH, Im H, Dahl JB. Non-contact microfluidic analysis of the stiffness of single large extracellular vesicles from idh1-mutated glioblastoma cells. *Adv Mater Technol*. 2023;8(7):2201412.
42. Anselmo AC, Zhang M, Kumar S, et al. Elasticity of nanoparticles influences their blood circulation, phagocytosis, endocytosis, and targeting. *ACS Nano*. 2015;9(3):3169–3177.
43. Ridolfi A, Brucale M, Montis C, et al. Afm-based high-throughput nanomechanical screening of single extracellular vesicles. *Anal Chem*. 2020;92(15):10274–10282.
44. Paolini L, Zendrini A, Radeghieri A. Biophysical properties of extracellular vesicles in diagnostics. *Biomarkers Med*. 2018;12(4):383–391.
45. Deserno M. Biomembranes balance many types of leaflet asymmetries. *Curr Opin Struct Biol*. 2024;87:102832.
46. Elani Y, Purushothaman S, Booth PJ, et al. Measurements of the effect of membrane asymmetry on the mechanical properties of lipid bilayers. *Chem Commun*. 2015;51:6976–6979.
47. Jo S, Kim T, Iyer VG, Im W. Charmm-gui: a web-based graphical user interface for charmm. *J Comput Chem*. 2008;29(11):1859–1865.
48. Wu EL, Cheng X, Jo S, et al. Charmm-gui membrane builder toward realistic biological membrane simulations. 2014.
49. Mark P, Nilsson L. Structure and dynamics of the tip3p, spc, and spc/e water models at 298 k. *J Phys Chem A*. 2001;105(43):9954–9960.
50. Abraham M, Alekseenko A, Bergh C, et al. Gromacs 2023.3 source code. 2023. http://dx.doi.org/10.5281/zenodo.10017686.
51. Klauda JB, Venable RM, Freites JA, et al. Update of the charmm all-atom additive force field for lipids: validation on six lipid types. *J Phys Chem B*. 2010;114(23):7830–7843.
52. Huang J, Rauscher S, Nawrocki G, et al. Charmm36m: an improved force field for folded and intrinsically disordered proteins. *Nature Methods*. 2017;14(1):71–73.
53. Jo S, Kim T, Im W. Automated builder and database of protein/membrane complexes for molecular dynamics simulations. *PloS One*. 2007;2(9):e880.
54. Parrinello M, Rahman A. Crystal structure and pair potentials: A molecular-dynamics study. *Phys Rev Lett*. 1980;45(14):1196.
55. Parrinello M, Rahman A. Polymorphic transitions in single crystals: A new molecular dynamics method. *J Appl Phys*. 1981;52(12):7182–7190.
56. Parrinello M, Rahman A. Strain fluctuations and elastic constants. *J Chem Phys*. 1982;76(5):2662–2666.
57. Feller SE, Zhang Y, Pastor RW, Brooks BR. Constant pressure molecular dynamics simulation: The langevin piston method. *J Chem Phys*. 1995;103(11):4613–4621.
58. Martyna GJ, Tobias DJ, Klein ML. Constant pressure molecular dynamics algorithms. *J Chem Phys*. 1994;101(4177):10–1063.
59. Darden T, York D, Pedersen L, et al. Particle mesh ewald: An n log (n) method for ewald sums in large systems. *J Chem Phys*. 1993;98. 10089–10089.
60. Piggot T, Allison J, Sessions R, Essex J. On the calculation of acyl chain order parameters from lipid simulations. *J Chem Theory Comput*. 2017;13:5683–5696.

61. Khelashvili G, Harries D. How cholesterol tilt modulates the mechanical properties of saturated and unsaturated lipid membranes. *J Phys Chem B*. 2013;117(8):2411–2421.
62. Khelashvili G, Johner N, Zhao G, Harries D, Scott H. Molecular origins of bending rigidity in lipids with isolated and conjugated double bonds: The effect of cholesterol. *Chem Phys Lipids*. 2014;178:18–26.
63. Watson MC, Brandt EG, Welch PM, Brown FLH. Determining biomembrane bending rigidities from simulations of modest size. *Phys Rev Lett*. 2012;109:028102.
64. Doktorova M, LeVine MV, Khelashvili G, Weinstein H. A new computational method for membrane compressibility: Bilayer mechanical thickness revisited. *Biophys J*. 2019;116(3):487–502.
65. Frenkel D, Smit B. *Understanding molecular simulation: from algorithms to applications*. Elsevier; 2023.
66. Janke W. Statistical analysis of simulations: Data correlations and error estimation. 2002:423–445. In: Quantum simulations of complex many-body systems: from theory to algorithms; vol. 10.